CORROSION CHALLENGES TOWARDS A SUSTAINABLE TURNING OF STAINLESS STEEL UNDER DIFFERENT COOLING METHODS

Graciela Šterpin Valić[1*] – Dario Kvrgić[2] – Goran Cukor[1] – Maja Vlatković[1]

[1]Department of Industrial Engineering and Management, Faculty of Engineering, University of Rijeka, Vukovarska 58, 51000 Rijeka, Croatia
[2]Department of Materials Engineering, Faculty of Engineering, University of Rijeka, Vukovarska 58, 51000 Rijeka, Croatia

ARTICLE INFO

***Article history*:**
Received: 03.10.2025.
Received in revised form: 09.10.2025.
Accepted: 09.10.2025.

Keywords:
Austenitic stainless steel
Vortex tube cooling
MQL
Corrosion performance

DOI: https://doi.org/10.30765/er.3074

Abstract:

Metalworking fluids are mostly produced based on mineral oils. Such fluids are not naturally biodegradable and contain large amounts of ingredients that are harmful to the environment and human health. They are therefore classified as hazardous waste and must be safely disposed of. Mineral oil-based fluids are the main unsustainable element of the metal cutting machining process. This study aims to investigate the influence of cutting parameters and cooling techniques (dry, conventional emulsion, minimum quantity lubrication (MQL), and MQL combined with vortex tube cooling) on the corrosion resistance of AISI 316L austenitic stainless steel. Electrochemical corrosion, and metallographic tests were performed. Surface chemical composition using energy-dispersive X-ray spectroscopy (EDS) before and after corrosion testing, and surface morphology using scanning electron microscopy (SEM) were analysed. The applied cooling method has a significant influence on both the elemental composition and the electrochemical behaviour of the machined surfaces. The role of machining-induced surface chemistry in localized corrosion behaviour is crucial. MQL-based techniques providing the most favourable electrochemical parameters and dry machining resulting in the poorest performance. The MQL combined with vortex tube cooling achieved the lowest corrosion rate (≈0.0308 mm/year), while dry machining exhibited the highest (≈0.0833 mm/year), highlighting the effectiveness of the hybrid sustainable cooling approach. The potential of MQL-based techniques as efficient and environmentally friendly alternatives to cooling has been confirmed.

1 Introduction

Conventional machining of stainless steels has long relied on mineral oil-based cutting fluids, primarily to extend tool life and maintain acceptable surface quality. Although technically effective, such fluids introduce a series of problems: they are expensive to produce, difficult to dispose of, and represent a major source of environmental and health hazards through soil and water contamination and the release of harmful aerosols [1,2]. Consequently, they are increasingly recognized as the least sustainable element of metal cutting operations [3]. The challenge of reducing this environmental burden has stimulated the search for alternative methods of cooling and lubrication, with the dual objective of safeguarding workers' health and lowering the ecological footprint of manufacturing processes. Austenitic stainless steel X2CrNiMo17-12-2 (AISI 316L) is one of the most widely applied materials in such processes. Its combination of mechanical strength,

* Corresponding author
E-mail address:graciela.sterpin@uniri.hr

weldability, and excellent resistance to general and localized corrosion explains its importance in industries as diverse as construction, biomedical engineering, and transport [2,4]. High chromium and molybdenum contents ensure improved protection against pitting in chloride-containing environments, whereas low carbon content minimizes carbide formation and preserves corrosion resistance [5]. Despite these advantages, machining of 316L is not straightforward: the material belongs to the group of difficult-to-cut alloys, in which tool wear and poor surface finish remain persistent issues unless effective cooling and lubrication are applied [6]. Despite their widespread application, conventional emulsion-based fluids derived from mineral oils are associated with severe ecological and health risks. Numerous studies emphasize that these fluids contribute to soil and water contamination and generate aerosols that are harmful to workers in machining environments [4]. Lawal [7] highlighted pollution of water, air, and soil, as well as contamination of agricultural products and food, and demonstrated the advantages of vegetable oil-based fluids used in MQL systems. Brinksmeier et al. [8] provided a comprehensive overview of cutting fluids, stressing both their technical benefits—such as extended tool life and improved surface finish—and their drawbacks, including pollution and health hazards. Schwarz et al. [9] discussed the impact of exposure to these fluids on workers, linking them to respiratory illnesses, allergies, skin disorders, and even cancer. In addition to health and environmental issues, Bierma and Waterstraat [10] pointed out that hidden costs of fluid usage can be several times higher than the purchase price. Finally, the environmental framework governing waste management also places increasing pressure on the use of such fluids.

These findings make clear that conventional emulsion fluids cannot be regarded as sustainable solutions for machining processes. Among the most frequently studied sustainable strategies are vortex tube cooling and minimum quantity lubrication (MQL). Vortex tubes generate a stream of cold air from compressed air, making it possible to reduce or completely avoid the use of conventional fluids [11]. MQL, on the other hand, provides only milliliters of biodegradable oil per hour in aerosol form, drastically lowering consumption while still supplying lubrication [12,13]. When these two approaches are combined, machining performance can be improved while ecological impact is minimized. Šterpin Valić et al. [12] demonstrated that the combination of biodegradable lubricants in MQL with vortex cooling substantially decreases the volume of fluid required and reduces environmental hazards, while other studies confirmed benefits in terms of tool life and surface finish [14]. The corrosion resistance of stainless steels is strongly influenced by the condition of the surface formed during machining, since corrosion processes are initiated at the surface rather than within the bulk material. Cooling conditions play an important role in defining these surface characteristics. Emulsion cooling has been reported to improve resistance by creating a lubricating film that protects the machined surface [15]. In contrast, cold compressed air supplied through vortex tube systems has been shown to lower cutting temperatures, which enhances surface quality and delays the onset of corrosion [16]. In addition, the surface chemistry is decisive for the early stages of corrosion: higher chromium and oxygen contents support the development of a stable, self-healing passive film, while carbon enrichment promotes chromium carbide formation that locally depletes protective elements and reduces the ability of the surface to resist corrosion [5]. SEM/EDS studies provide detailed evidence of how specific surface heterogeneities influence localized corrosion in stainless steels. Matula et al. [1] demonstrated that chromium depletion along grain boundaries in 316L promotes intergranular corrosion, illustrating the role of selective chemical variations. DelVecchio et al. [17] reported that microsegregation of chromium and molybdenum in additively manufactured 316L facilitates local breakdown of passivity, while Zhang et al. [18] linked MnS inclusions in 304 stainless steel to pit initiation. Burstein & Pistorius [19] further emphasized the influence of surface condition, noting that smoother surfaces show fewer but more stable pits. Although focused on different alloys and corrosion types, these studies consistently demonstrate that localized modifications of the surface determine where corrosion initiates and how it propagates. Surface condition created during machining is another decisive factor for corrosion resistance. De Oliveira Jr. et al. [20] showed that tool wear and surface roughness in the turning of super duplex stainless steel are closely correlated with corrosion performance, while Bueno et al.

[21] demonstrated that increased roughness in super martensitic stainless steel enhances susceptibility to pitting in seawater. Complementary findings were reported by Cukor et al. [22], who observed that vortex tube cooling not only avoids negative effects on corrosion resistance of martensitic stainless steel but even produces surfaces with higher chromium and lower carbon contents, thus providing more favorable conditions for passivity. Despite these advances, a clear research gap remains. While the individual benefits of MQL and vortex tube cooling are documented, their combined effect on the corrosion resistance of machined AISI 316L has not been fully clarified [4,12]. To address this, the present study examines the corrosion behavior of 316L

under four machining conditions: dry cutting, conventional emulsion, MQL, and MQL with vortex tube cooling. By applying electrochemical testing, metallographic evaluation, and SEM/EDS analyses, this research seeks to identify which cooling strategy provides the best balance between environmental sustainability and corrosion resistance. The findings are expected to strengthen the case for MQL-based methods as viable, environmentally friendly alternatives to conventional flood cooling in the machining of stainless steels.

2 Materials and Methods

2.1 Material

The investigated material was austenitic stainless steel X2CrNiMo17-12-2 (AISI 316L), supplied in the form of cylindrical rods with a diameter of 85 mm and a length of 530 mm. For all machining trials, a longitudinal turning length of 460 mm was selected. From the machined rods, small discs with a diameter of 16 mm and a thickness of 4 mm were prepared. For each cooling method, three discs were produced and subsequently subjected to corrosion testing. The bulk chemical composition of the base material was determined using a glow discharge optical emission spectrometer (LECO GDS500A), Table 1.

Table 1. Chemical composition of the base material, measured by GDS500A spectrometer.

Element	**Cr**	**Ni**	**Mn**	**Si**	**C**	**S**	**Fe**
wt. %	15.8 %	10.5 %	1.96 %	0.555 %	0.0001 %	0.0311 %	67.4 %

2.2 Machining Procedure

Machining experiments were performed on a CNC lathe TU 360 Prvomajska, equipped with Seco turning inserts DNMG 150608-MF4, grade TM3501, and a Seco tool holder DDJNL 2525M15-M, Figure 1. Constant cutting parameters were applied across all tests: cutting speed v_c= 60 m/min, feed rate f = 0.22 mm/rev, and depth of cut a_p= 1.3 mm.

Four different cooling and lubrication strategies were applied during machining:

- Dry machining (no cooling) – baseline condition without external cooling or lubrication.
- Conventional emulsion cooling – using INA BU 7 emulsifying concentrate prepared with water.
- Minimum Quantity Lubrication (MQL) – applied via an SKF VE1B unit with the integrated tank capacity of 0.3 l, air flow at 6 bar is 170 l/min, micropump delivery rate from 7 to 30 mm3/stroke, pump working frequency is 1 strokes/s, using biodegradable LUB 200 oil composed of natural triglycerides and refined rapeseed oil.
- MQL combined with vortex tube cooling (MQL + VC) – integration of the MQL system with an EXAIR counter-flow vortex tube (model 3825) with an air flow of 708 l/min, inlet air pressure of 0.69 MPa and cooled air temperature of −8 °C, delivering compressed cold air simultaneously with lubricant, Figure 1.

Figure 1. a) CNC Lathe TU 360 Prvomajska, b) MQL and vortex tube, c) Integrated MQL/VC system.

2.3. Surface Characterization

Roughness Measurement

Surface roughness of the machined samples was measured using a Hommel Tester T1000 (JENOPTIK, Germany). For each sample, at least three measurements were recorded, and the average values of *Ra* and *Rz* parameters were calculated.

SEM/EDS Analysis

Detailed morphological and compositional analysis was carried out using scanning electron microscopy (SEM) coupled with energy-dispersive spectroscopy (EDS). A JEOL JSM-7800F microscope equipped with an Oxford Instruments X-MaxN80 EDS detector was employed for these analyses, Figure 2. Surface characterization was performed both before corrosion testing (to evaluate machining-induced conditions) and after exposure (to assess localized damage and compositional changes). After corrosion, three characteristic zones were examined: (i) unaffected surface regions, (ii) pit edges, and (iii) pit bottoms, with at least three measurements taken for each zone.

Figure 2. SEM/EDS analysis device.

2.4 Corrosion Testing

Electrochemical Measurements

Electrochemical tests were carried out using a Gamry Interface 1010E potentiostat in a conventional three-electrode configuration, consisting of the machined steel sample as the working electrode, an Ag/AgCl (3 M KCl) reference electrode placed in a Luggin capillary, and a platinum mesh counter electrode, Figure 3. The electrolyte was a 3.5 wt.% NaCl aqueous solution at 25 ± 1 °C. Prior to testing, sample surfaces were rinsed with deionized water and ethanol. The exposed surface area of each specimen was precisely defined at 1.0 cm^2 using a specialized sample holder that allowed contact with the electrolyte only on a single circular face of the

disc. All electrochemical measurements were performed under naturally aerated conditions at 25 ± 1 °C to simulate realistic oxygenated saline exposure. To minimize the uncompensated solution resistance (iR drop), a Luggin capillary was positioned with its tip approximately 1–2 mm from the working electrode surface, ensuring accurate potential control during all measurements.

The following procedures were applied:

- Open Circuit Potential (*OCP*): monitored for 1 h to evaluate passive film stabilization.
- Linear Polarization Resistance (*LPR*): performed in the potential range ±20 mV vs. *OCP* at a scan rate of 0.167 mV/s, to determine polarization resistance (*Rp*).
- Potentiodynamic Polarization (PDP): measured from −250 mV to +1000 mV vs. *OCP* at a scan rate of 0.5 mV/s, to determine corrosion potential (E_{corr}), corrosion current density (i_{corr}), and pitting potential (E_p).

Gravimetric Measurements

In parallel with electrochemical testing, immersion experiments were performed for long-term evaluation. Samples were fully immersed in a 3.5 wt.% NaCl solution at 25 ± 1 °C for a total duration of 28 days, Figure 3. At intervals of 7, 14, 21, and 28 days, the specimens were removed, cleaned to remove corrosion products, dried, and weighed using a precision balance (±0.1 mg). Mass loss values (Δm) were used to calculate average corrosion rates.

Figure 3. Electrochemical test setup with Gamry Interface 1010E potentiostat and Gravimetric setup with 316L steel samples immersed in 3.5 wt.% NaCl solution.

3 Results

3.1 Corrosion Testing

3.1.1 Open Circuit Potential (OCP)

The results of open circuit potential (*OCP*) measurements for 316L steel machined under different cooling conditions are presented in Table 2. The measurements were conducted for a duration of 1 h in a 3.5 % NaCl solution to simulate seawater exposure. During the OCP test, the potential difference (V vs. Ag/AgCl) between the working electrode (316L steel) and the reference electrode was continuously monitored to evaluate the electrochemical stability of the steel under the applied cooling conditions.

Table 2. Open circuit potential (OCP) values of 316L steel under different cooling conditions.

Cooling Medium	Final open circuit potential (V)
Dry machining	-0.0818
Emulsion	-0.0438
MQL	-0.0750
MQL combined with vortex	-0.0266

The open circuit potential varied considerably depending on the applied cooling strategy. In the dry condition, the potential stabilized at −0.0818 V, serving as a baseline for the material's electrochemical behavior without external cooling or lubrication. Emulsion cooling significantly improved performance, yielding a final *OCP* of −0.0438 V, which indicates a more favorable stabilization of the passive film [15]. Minimum quantity lubrication (MQL) resulted in a final potential of −0.0750 V, slightly better than dry cutting but inferior to emulsion. The best response was obtained under combined MQL and vortex tube cooling, with a final potential of −0.0266 V, reflecting the strongest stabilization of the electrochemical interface. In terms of time-dependent behavior, differences in stability were also observed. MQL exhibited the lowest fluctuation of *OCP* values, suggesting stable electrochemical conditions throughout the test. Conversely, emulsion cooling showed the most unstable potential evolution, indicating that the protective film formed on the surface was less consistent during exposure. The combination of MQL with vortex tube cooling provided both strong stabilization of the final potential and moderate time stability, highlighting the synergistic effect of simultaneous lubrication and efficient thermal management [15].

3.1.2 Linear Polarization Resistance (LPR)

Polarization resistance (R_p) is a critical parameter for evaluating the corrosion resistance of stainless steel, as it provides a quantitative measure of how processing conditions influence electrochemical stability. The results of linear polarization tests for 316L steel under different cooling strategies are summarized in Table 3. Dry machining material exhibited an R_p of 17.29 kΩ, representing the reference value for the alloy in the absence of external cooling or lubrication. Emulsion cooling substantially improved corrosion resistance, reaching 25.49 kΩ, which confirms the protective effect of a lubricating film formed during machining. In contrast, minimum quantity lubrication (MQL) produced the lowest R_p of 11.26 kΩ, indicating reduced resistance to corrosion despite the environmental and economic benefits of this method. The combination of MQL with vortex cooling yielded an R_p of 24.98 kΩ, nearly matching the performance of emulsion cooling. This result highlights the synergistic effect of combining minimal lubrication with enhanced cooling, which provides improved stabilization of the passive film. Overall, these findings demonstrate that while emulsion cooling ensures the highest resistance to corrosion, MQL combined with vortex cooling offers a comparable level of protection and represents a promising sustainable alternative [23].

Table 3. Polarization resistance (R_p) values of 316L steel under different cooling conditions.

Cooling Medium	Polarization resistance (kΩ)
Dry machining	17.29
Emulsion	25.49
MQL	11.26
MQL combined with vortex	24.98

3.1.3 Potentiodynamic Polarization (PDP)

The potentiodynamic polarization method is a powerful tool for investigating corrosion mechanisms, electrode reaction kinetics, and the resistance of materials in aggressive electrolytes. For the 316L steel, the polarization curves obtained under different cooling strategies exhibited a consistent progression from cathodic oxygen reduction to anodic oxidation and subsequent passivation (Figure 4). With further potential increase, the passive film eventually breaks down at the pitting potential (E_p), resulting in a sharp rise in current density, which marks the onset of localized corrosion [24]. The quantitative results are summarized in Table 4.

Table 4. Potentiodynamic polarization parameters of 316L steel under different cooling conditions.

Cooling Medium	Corrosion current density (i_{corr}/μA)	Corrosion potential (E_{corr}/mV)	Pitting potential (E_p/V)	Corr. rate (mm/year)
Dry machining	0.883	34.66	0.3491	90.95
Emulsion	1.784	-29.15	0.2843	41.72
MQL	1.445	-57.86	0.2916	33.73
MQL combined with vortex	1.388	-19.33	0.3041	33.66

The dry machining material exhibited an i_{corr} of 0.883 μA and an E_{corr} of +34.66 mV, with a calculated corrosion rate of 0.09095 mm/year. The corrosion rate (CR) was automatically calculated by the Gamry Echem Analyst software based on the corrosion current density (i_{corr}) determined from Tafel extrapolation. The calculation follows Faraday's law according to the relation:

$$CR\ (\mathrm{mm/year}) = 0.00327\ \times i_{corr}(\mu A/cm^2) \times \frac{EW}{\rho} \tag{1}$$

Where EW is the alloy equivalent weight derived from the nominal chemical composition (Table 1), and ρ is the density of 316L stainless steel. This condition serves as a reference for evaluating the influence of cooling and lubrication. Emulsion cooling showed a shift of E_{corr} towards −29.15 mV and a reduction in the corrosion rate to 0.04172 mm/year, reflecting the formation of a more protective passive layer despite an increase in i_{corr}. The MQL condition further lowered the corrosion rate to 0.03373 mm/year, representing an improvement over both dry and emulsion machining. The most favorable results were obtained under MQL combined with vortex tube cooling, with i_{corr} reduced to 1.388 μA, E_{corr} shifted to −19.33 mV, and a corrosion rate of 0.03366 mm/year. This confirms the synergistic effect of minimal lubrication and intensive cooling, yielding corrosion resistance nearly identical to emulsion cooling while offering a more sustainable solution.

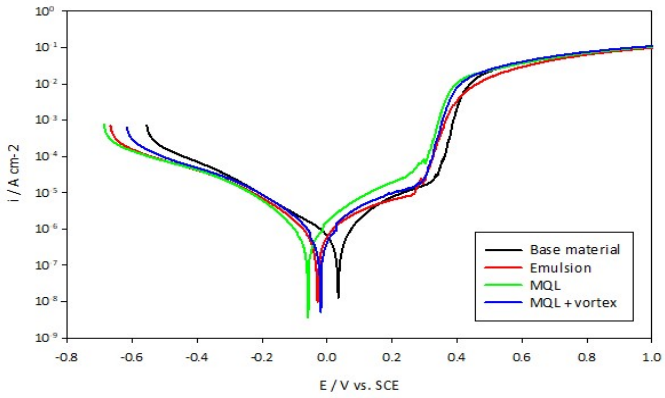

Figure 4. Potentiodynamic polarization curves of 316L steel under different cooling conditions.

Gravimetric Testing.

Gravimetric measurements were performed on 316L steel samples machined under different cooling conditions and subsequently immersed in a 3.5 % NaCl solution for a period of 28 days. At weekly intervals, the samples were removed, cleaned of corrosion products, dried, and reweighed to determine the mass loss (Δm). The cleaning procedure followed the general recommendations of ASTM G1-03 for stainless steels, employing rinsing with demineralized water and gentle ultrasonic cleaning to remove corrosion products without altering the underlying metallic surface.

The obtained values are presented in Table 5.

Table 5. Gravimetric measurements of sample masses and mass changes.

Sample	Mass day 0 (g)	Mass day 7 (g)	Δm_1(g)	Mass day 14 (g)	Δm_2(g)	Mass day 21 (g)	Δm_3(g)	Mass day 28 (g)	Δm_4(g)
Dry machining	5.3811	5.3805	0.0006	5.3799	0.0012	5.3792	0.0019	5.3784	0.0027
Emulsion	5.3033	5.3030	0.0003	5.3027	0.0006	5.3022	0.0011	5.3019	0.0014
MQL	5.3018	5.3016	0.0002	5.3012	0.0006	5.3010	0.0008	5.3006	0.0012
MQL combined with vortex	5.3327	5.3325	0.0002	5.3322	0.0005	5.3319	0.0008	5.3317	0.0010

The progressive decrease in mass over time provided the basis for calculating the corrosion rates at each interval. The corrosion rate (CR) was determined from the measured mass loss according to the relation:

$$CR\ (\text{mm/year}) = \frac{8.76 \times 10^4 \times\ \Delta m}{\rho\ \times A \times t} \tag{2}$$

Where Δm is the mass loss (g), ρ is the material density (g/cm³), A is the exposed surface area (cm²), and t is the exposure time (h). The constant 8.76×10^4 converts the rate to millimetres per year.

These results are summarized in Table 6. To provide a more comprehensive view of corrosion behavior, gravimetric results were compared with corrosion rates determined by electrochemical measurements. The comparison is shown in Table 7 and Figure 5.

Table 6. Corrosion rates of samples over time by gravimetric method.

Sample	Corrosion rate day 7 (mm/year)	Corrosion rate day 14 (mm/year)	Corrosion rate day 21 (mm/year)	Corrosion rate day 28 (mm/year)
Dry machining	0.0740	0.0740	0.0781	0.0833
Emulsion	0.0370	0.0370	0.0452	0.0432
MQL	0.0247	0.0370	0.0329	0.0370
MQL combined with vortex	0.0247	0.0308	0.0329	0.0308

Table 7. Comparison of corrosion rates obtained by gravimetric and electrochemical methods.

Sample	Gravimetric Corrosion Rate (mm/year)	Electrochemical Corrosion Rate (mm/year)
Dry machining	0.0833	0.09095
Emulsion	0.0432	0.04172
MQL	0.037	0.03373
MQL combined with vortex	0.0308	0.03366

Both methods showed that the dry machining material had the highest corrosion rates (0.0833 vs. 0.09095 mm/year), with small differences explained by the cumulative nature of gravimetric versus instantaneous electrochemical testing [24]. Emulsion cooling reduced the rate to about 0.043 mm/year in both methods, while MQL lowered it further to ~0.037/0.034 mm/year. The best performance was obtained with MQL combined with vortex cooling (0.0308 vs. 0.0337 mm/year), confirming the consistency of the two techniques and the effectiveness of this hybrid approach.

Figure 5. Comparison of corrosion rates from gravimetric (green) and electrochemical (blue) measurements.

3.2 Surface Characterization

3.2.1 Surface Roughness after Machining

Surface roughness is an important factor influencing the corrosion behaviour of stainless steel, as it affects both passive film stability and the tendency toward localized corrosion. The parameters *Ra* (arithmetic average roughness) and *Rz* (average maximum profile height) are commonly used to describe the quality of machined surfaces [4].

Table 8. Surface roughness parameters Ra and Rz for 316L steel under different cooling conditions.

Cooling Medium	***Rz* (µm)**	***Ra* (µm)**
Dry machining	2.2700	0.5525
Emulsion	2.3950	0.4415
MQL	3.9250	0.7425
MQL combined with vortex	4.0600	0.8417

As shown in Table 8, emulsion cooling produced the smoothest surface, while MQL and MQL combined with vortex cooling led to noticeably higher roughness values. Dry machining resulted in intermediate roughness, falling between emulsion and the MQL-based strategies. These results confirm that sustainable cooling approaches may sacrifice some surface finish quality compared to conventional emulsion. However, roughness alone does not fully explain the observed electrochemical behaviour, as seen in the *OCP* measurements, where emulsion provided the lowest roughness but not the most stable potential.

3.2.2 Optical Microscopy Before and After Corrosion

Optical microscopy provided a macroscopic assessment of the machined surfaces before and after electrochemical testing, as shown in Figure 6. Before corrosion, all samples displayed a comparable surface appearance. Characteristic machining marks from the turning process were clearly visible, but no deviations such as pores, cavities, or irregularities were observed. This confirms that the machining and cooling procedures did not introduce significant surface defects at the optical scale. After potentiodynamic

measurements, however, distinct signs of localized corrosion were apparent. Small, discrete pits formed on the surfaces of all samples, confirming the onset of pitting corrosion. These visual findings are consistent with the electrochemical data, providing complementary evidence of localized attack in chloride solution.

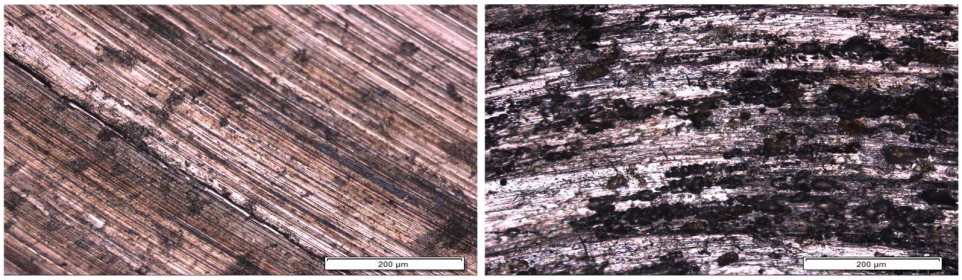

a) *b)*

Figure 6. Optical microscopy images of 316L steel samples before (a) and after (b) potentiodynamic measurements, 10× magnification.

3.2.3 SEM Analysis Before and After Corrosion

Scanning electron microscopy (SEM) was employed to investigate the surface morphology of X2CrNiMo17-12-2 stainless steel before and after corrosion testing. After exposure, the corroded surface was further examined in three characteristic zones: the unaffected surface, the pit edge, and the pit bottom. Representative SEM images with corresponding EDS spectra illustrating the pre-corrosion surface, post-corrosion surface region, pit edge, and pit bottom are presented in Figures 7–10. Before corrosion, the surface exhibited a uniform machined texture, characterized by grooves and ridges resulting from the turning process. No indications of corrosion damage were observed at this stage, confirming the integrity of the as-machined surface.

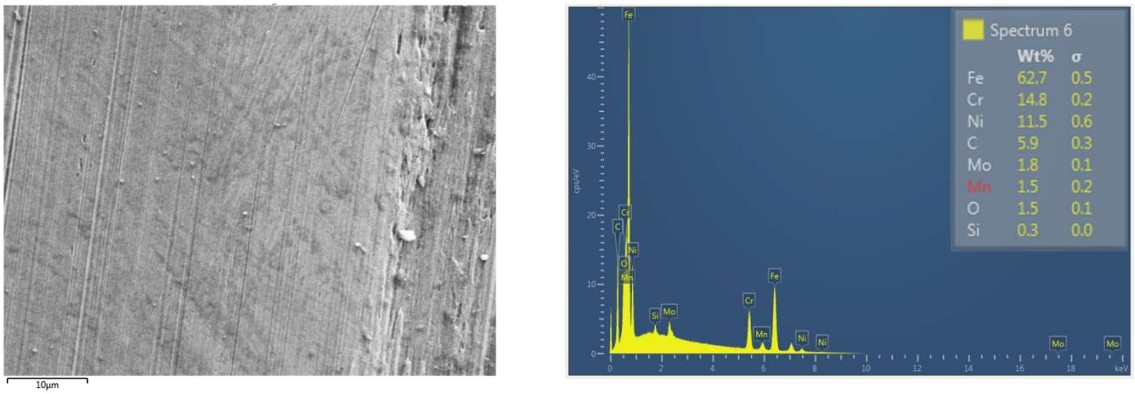

Figure 7. SEM image of the pre-corrosion surface of 316L steel with corresponding EDS spectrum.

Following corrosion testing, SEM analysis revealed that large portions of the surface remained visually similar to the pre-corrosion condition, still dominated by machining marks. No widespread degradation was observed, indicating that corrosion processes did not affect the entire surface uniformly. These findings are consistent with optical microscopy results, which also showed largely unchanged surfaces with the appearance of localized pits after testing.

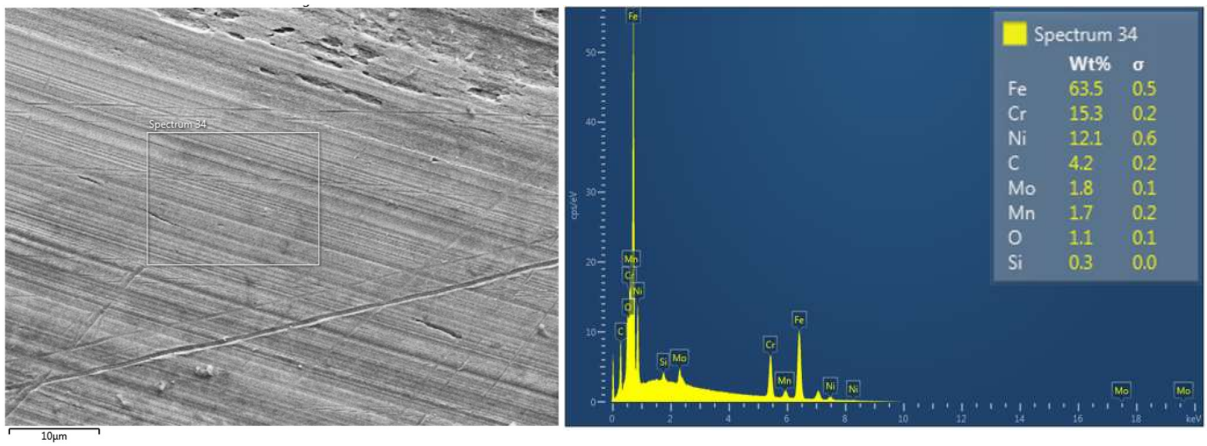

Figure 8. SEM image of the post-corrosion surface region of 316L steel with corresponding EDS spectrum.

The pit edge showed a distinct morphological transition between intact and corroded regions. This area displayed visible roughening and breakdown of the surface, highlighting the localized initiation of corrosion.

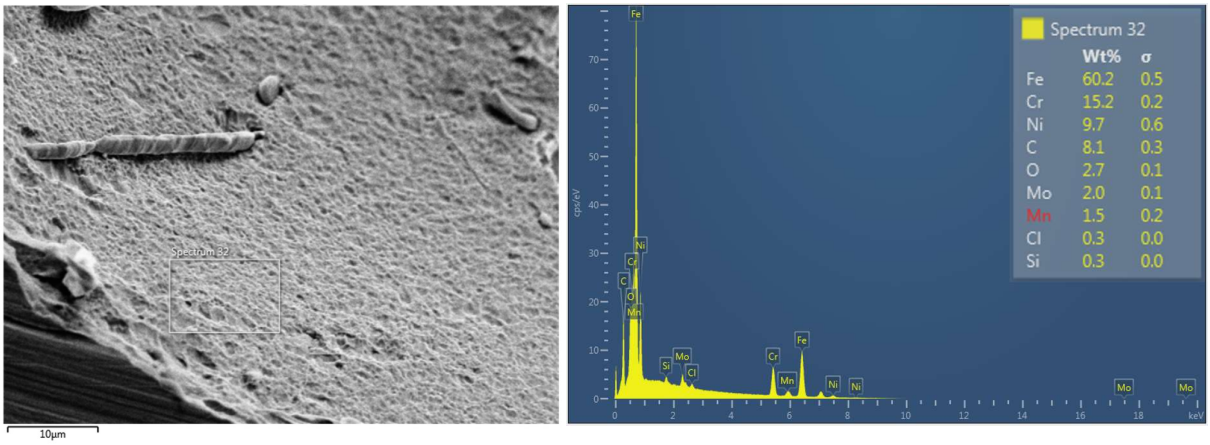

Figure 9. SEM image of the pit edge region of 316L steel after corrosion testing with corresponding EDS spectrum.

The most severe changes were observed at the pit bottom. Here, the original machining pattern was completely lost, and the surface appeared highly irregular, with pronounced roughness and dissolution features. This morphology is consistent with advanced stages of localized corrosion, where the passive layer has been fully disrupted and material loss is most significant.

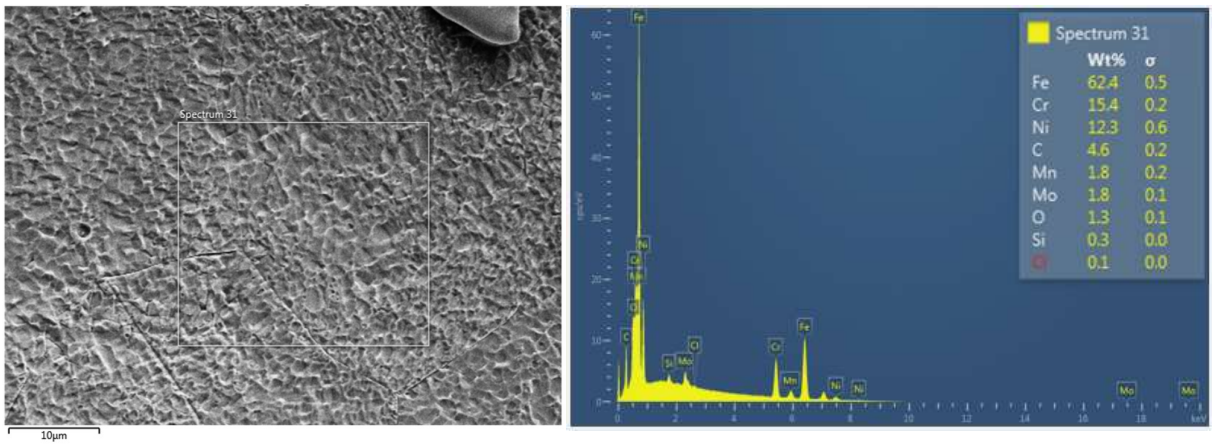

Figure 10. SEM image of the pit bottom region of 316L steel after corrosion testing with corresponding EDS spectrum.

3.2.4 EDS Analysis

The surface chemical composition of X2CrNiMo17-12-2 stainless steel samples was examined using energy-dispersive spectroscopy (EDS). The analysis was carried out to determine how machining under different cooling conditions affected the elemental distribution on the surface, and how these differences influenced corrosion resistance. Measurements were performed both before and after corrosion testing. After corrosion, the analysis focused on three characteristic zones: the unaffected surface, the pit edge, and the pit bottom, to capture chemical differences associated with localized corrosion processes.

EDS Before Corrosion

The pre-corrosion analysis revealed that iron (Fe) remained the dominant element across all conditions, while chromium (Cr), nickel (Ni), carbon (C), and oxygen (O) showed significant variations depending on the applied cooling strategy. Results are presented in Table 9.

Table 9. Surface chemical composition of 316L steel samples before corrosion testing under different cooling conditions.

Cooling Medium	Fe (wt. %)	C (wt. %)	Cr (wt. %)	Ni (wt. %)	O (wt. %)	Mn (wt. %)	Mo (wt. %)	Si (wt. %)	S (wt. %)	Ca (wt. %)	Al (wt. %)
Dry machining	62.78	5.36	15.12	12.02	0.78	1.18	1.02	0.30	0.04	0.04	0
Emulsion	62.10	6.14	14.70	11.90	1.42	1.28	1.76	0.26	0	0.02	0.02
MQL	62.76	14.94	14.26	9.28	1.58	1.36	1.10	0.30	0.08	0.10	0.02
MQL combined with vortex	61.70	8.94	14.36	9.66	1.58	1.24	1.00	0.28	0	0	0

Dry machining samples exhibited the highest Cr and Ni contents, together with the lowest oxygen fraction, suggesting limited oxide formation and weaker initial passivation [8]. In contrast, the MQL condition led to a

sharp increase in carbon, attributed to lubricant residues. Emulsion and MQL + vortex conditions showed moderate carbon levels, indicating partial contamination but also more effective removal of residues. Oxygen was consistently higher in lubricated samples, especially under MQL and MQL + vortex, pointing to enhanced oxide formation during machining. Molybdenum and manganese showed moderate increases, while trace elements such as sulphur, calcium, and aluminium were detected without a consistent trend [25].

EDS After Corrosion

Following corrosion exposure in a 3.5 % NaCl solution, localized surface degradation occurred, resulting in the formation of corrosion pits. To assess chemical changes induced by electrochemical processes, EDS analysis was performed on three characteristic surface regions: the unaffected surface, the pit edge, and the pit bottom. This approach enables a detailed understanding of the redistribution of alloying elements and the selective loss of protective components depending on the corrosion location [26]. The distribution of elements across the surface regions after corrosion followed the same pattern observed in optical and SEM images: the general surface remained relatively intact, the pit edge represented a transitional area, while the pit bottom exhibited the most severe degradation.

i.) Surface region

The surface region, representing areas unaffected by visible pits, displayed noticeable changes in chemical composition compared to the pre-corrosion state. The results are summarized in Table 10.

Table 10. Surface chemical composition of 316L steel samples after corrosion testing under different cooling conditions – Surface region.

Cooling Medium	Fe (wt. %)	C (wt. %)	Cr (wt. %)	Ni (wt. %)	O (wt. %)	Mn (wt. %)	Mo (wt. %)	Si (wt. %)	S (wt. %)	Cl (wt. %)	Na (wt. %)
Dry machining	64.67	12.83	15.30	11.83	1.40	1.70	1.17	0.27	0.00	0.00	0.00
Emulsion	63.80	8.24	15.44	11.48	1.42	1.82	1.82	0.30	0.00	0.08	0.12
MQL	64.00	13.57	12.10	10.43	1.80	1.57	0.83	0.30	0.00	0.00	0.00
MQL combined with vortex	64.08	3.74	15.24	12.56	0.80	1.48	1.30	0.28	0.04	0.00	0.00

The most significant differences were observed in chromium, nickel, molybdenum, and carbon content. Samples machined under the MQL condition exhibited the lowest chromium (12.10 wt.%) and nickel (10.43 wt.%). In contrast, emulsion and MQL + vortex methods preserved higher concentrations of these elements, with nickel in MQL + vortex even exceeding pre-corrosion values, suggesting heterogeneous redistribution during electrochemical attack and possible local enrichment effects [19]. Carbon remained elevated under MQL (13.57 wt.%), confirming persistent contamination from lubricant residues [8]. Conversely, in the MQL + vortex condition, carbon content decreased to 3.74 wt.%, likely due to partial removal of organic residues by the turbulent airflow [8,19]. Oxygen content increased in most conditions, especially in MQL (1.80 wt.%), indicating oxide formation during exposure [27]. Molybdenum reached its highest concentration in emulsion-treated samples (1.82 wt.%), which may contribute to better stability of the passive film under these conditions [28].

i.) Pit edge region

The pit edge represents the transitional region between the intact surface and the severely degraded pit bottom. EDS analysis revealed intermediate values for both alloying elements and contaminants, reflecting the progressive redistribution of elements under localized electrochemical activity [28]. The results are summarized in Table 11.

Table 11. Surface chemical composition of 316L steel samples after corrosion testing under different cooling conditions – Pit edge region.

Cooling Medium	Fe (wt. %)	C (wt. %)	Cr (wt. %)	Ni (wt. %)	O (wt. %)	Mn (wt. %)	Mo (wt. %)	Si (wt. %)	S (wt. %)
Dry machining	60.25	9.63	18.58	11.03	1.48	2.10	0.90	0.20	0.18
Emulsion	65.28	2.79	17.76	7.43	1.00	2.39	0.50	0.22	0.13
MQL	63.57	10.60	16.43	11.45	2.52	2.27	0.97	0.25	0.00
MQL combined with vortex	55.80	11.28	15.78	10.60	2.75	1.95	1.30	0.25	0.18

Chromium and nickel contents at the pit edge were in most cases comparable or slightly higher than on the unaffected surface, suggesting partial retention of passivating elements despite ongoing corrosion. For instance, the dry machining material showed Cr = 18.58 wt.% and Ni = 11.03 wt.%, with chromium notably higher than at the surface, indicating possible enrichment through selective dissolution [27]. In contrast, the emulsion-treated sample exhibited reduced values (Cr = 17.76 wt.%, Ni = 7.43 wt.%), pointing to a more advanced depletion of passivating species in this region [28]. Carbon remained elevated across all conditions, particularly in MQL (10.60 wt.%) and MQL + vortex (11.28 wt.%), consistent with residual lubricant and partially oxidized degradation products [8,18]. The dry machining material also displayed a relatively high carbon level (9.63 wt.%), which can be linked to the lack of flushing during machining, allowing adsorption of organic residues and thermal accumulation. Such deposits may hinder the removal of contaminants and contribute to surface instability at the pit edge. Oxygen content increased compared to the surface region, ranging from 1.00 to 2.75 wt.%. The highest values were observed for MQL (2.52 wt.%) and MQL + vortex (2.75 wt.%), reflecting enhanced oxide formation at the onset of passive film breakdown [27]. This gradual oxygen enrichment from surface to pit edge, and further to pit bottom, correlates with intensifying electrochemical activity and loss of passivation [25]. The pit edge region therefore represents an electrochemically unstable interface, where early signs of localized corrosion and passive film degradation are clearly manifested. Its intermediate composition reflects both the influence of machining conditions and the spatial progression of corrosion [28].

i.) Pit bottom region

At the bottom of the pits, the EDS results showed the most pronounced deviations in chemical composition, reflecting the severity of localized degradation. The results are summarized in Table 12.

Table 12. Surface chemical composition of 316L steel samples after corrosion testing under different cooling conditions – Pit bottom zone.

Cooling Medium	Fe (wt. %)	C (wt. %)	Cr (wt. %)	Ni (wt. %)	O (wt. %)	Mn (wt. %)	Mo (wt. %)	Si (wt. %)	S (wt. %)	Cl (wt. %)
Dry machining	55.13	11.83	14.03	7.20	0.60	1.27	0.67	0.37	0.00	0.20
Emulsion	65.95	1.25	15.85	10.15	0.35	1.70	1.55	0.25	0.00	0.10
MQL	61.60	8.27	14.53	9.40	1.87	1.53	0.90	0.37	0.00	0.17
MQL combined with vortex	0.78	51.34	0.28	0.00	24.22	0.00	0.00	0.02	1.26	1.54

Note:

For the first three cooling conditions, the total elemental sum is close to 100 wt.% because only elements with relevant and consistent signal intensities were considered, while minor artefactual peaks (<0.5 wt.%) were excluded. In contrast, for the MQL + vortex condition, the total sum is lower (≈79 wt.%) due to the appearance of an additional low-energy peak attributed by the software to nitrogen (≈17 wt.%). Since nitrogen is not expected in the system and was not detected under any other condition, this value is considered an analytical artefact related to signal distortion and poor detection geometry at the pit bottom. Compared with the pit edge and unaffected surface, the pit bottom was characterized by a substantial depletion of passivating elements and a concurrent accumulation of corrosion-related products, confirming the collapse of the protective film and loss of electrochemical stability [27,28]. Iron content dropped dramatically in the MQL + vortex condition, reaching only 0.78 wt.%. Such an unrealistically low value likely reflects analytical artefacts caused by severe pitting or poor signal quality in deep cavities. In contrast, emulsion-treated samples retained high Fe content (65.95 wt.%), suggesting a better-preserved metallic matrix. Chromium and nickel followed a similar trend. The MQL + vortex sample showed extreme depletion (Cr = 0.28 wt.%, Ni = 0.00 wt.%), whereas more stable levels were observed in the emulsion (Cr = 15.85 wt.%, Ni = 10.15 wt.%) and MQL (Cr = 14.53 wt.%, Ni = 9.40 wt.%) conditions.

The dry machining sample also displayed strong reductions, confirming substantial loss of corrosion-resistant alloying elements [27,28]. Oxygen content increased sharply in the MQL + vortex sample (24.22 wt.%), indicating extensive oxide formation. Carbon content also peaked under the same condition (51.34 wt.%), far exceeding all other cases. This suggests either massive accumulation of lubricant residues or interference from non-metallic deposits [8,28]. Conversely, emulsion-treated samples displayed the lowest carbon values (1.25 wt.%), consistent with cleaner surfaces and more stable chemistry. Molybdenum was best preserved in the emulsion condition (1.55 wt.%), supporting its role in localized corrosion resistance [28]. Manganese and silicon showed moderate values in most cases, but Mn was completely absent in the MQL + vortex condition, further suggesting unreliable quantification in severely corroded cavities. Chloride and sulphur were detected only in trace amounts, but their highest levels occurred in the MQL + vortex sample (Cl = 1.54 wt.%, S = 1.26 wt.%), reflecting entrapment of electrolyte and aggressive anions [19]. Overall, the pit bottom region represents the most chemically altered part of the surface, marked by depletion of key alloying elements and accumulation of oxides, carbonaceous residues, and chloride species. In the MQL + vortex condition, the Fe and Cr contents at the pit bottom were extremely low, while C was abnormally high. These deviations are consistent with previously reported findings and are most likely caused by analytical artefacts related to the deep pit geometry and reduced signal intensity. Therefore, EDS quantification in this region should be interpreted with caution, as it may not accurately represent the true elemental composition. These results highlight both the severity of localized attack and the potential analytical limitations of EDS when measuring extreme pit environments.

3.3 Correlation

The correlation analysis was conducted to establish quantitative relationships between electrochemical parameters and surface characteristics. Pearson's correlation coefficient was applied [29,11], enabling the identification of trends between local composition, roughness, and electrochemical behaviour. Positive values ($r > 0$) indicate a direct association between elemental concentration and electrochemical response, while negative values ($r < 0$) reflect an inverse trend. Correlation strength is classified as weak ($|r| < 0.5$), moderate ($0.5 \leq |r| < 0.8$), or strong ($|r| \geq 0.8$). This framework enables the identification of compositional or topographical features that enhance passivation or accelerate degradation [1,19].

i.) Correlation before corrosion

To investigate the influence of initial surface chemistry and roughness on corrosion resistance, Pearson correlation coefficients were calculated between the elemental composition before corrosion and two key electrochemical parameters, *OCP* and *Rp*, together with *Ra* and *Rz* roughness descriptors [8]. A visual representation of these relationships is provided in the bar chart of Figure 11, which further highlights elements and surface features with positive and negative contributions to early-stage passivation.

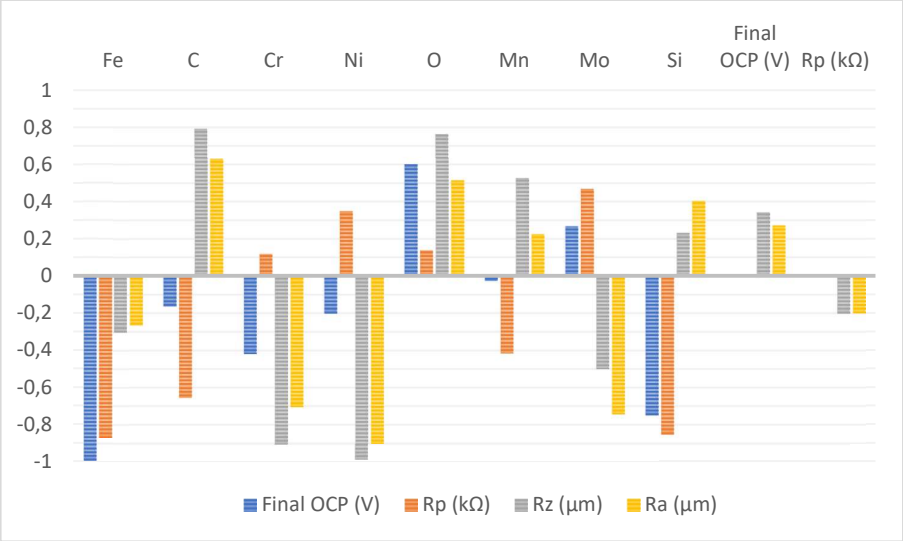

Figure 11. Bar chart of correlations between surface features and electrochemical parameters before corrosion.

The results revealed a very strong negative correlation between Fe and *OCP* (r = −0.99), confirming that surface enrichment with the base metal shifts the potential towards more active values. Si also showed a strong negative effect (r = −0.75), while Cr (r = −0.42) and Ni (r = −0.20) exhibited weaker negative trends. In contrast, O correlated positively with OCP (r = 0.60), linking oxygen enrichment to more noble behaviour, whereas Mo displayed only a weak positive influence (r = 0.27). Mn showed no relevant relationship with OCP (r = −0.03). For *Rp*, the strongest negative correlations were observed for Fe (r = −0.87), Si (r = −0.86) and C (r = −0.66), indicating that higher fractions of these elements reduce polarization resistance. Ni (r = 0.35) and Mo (r = 0.47) showed moderate positive correlations, while Cr (r = 0.12) and O (r = 0.14) were only weakly positive. Mn exhibited a moderate negative correlation (r = −0.42), suggesting a detrimental effect at higher surface concentrations. In terms of surface roughness, both *Ra* and *Rz* correlated strongly and positively with C (*Ra* r = 0.63; *Rz* r = 0.79) and O (*Ra* r = 0.51; *Rz* r = 0.76), suggesting that their enrichment is linked to rougher surfaces. Conversely, Ni (*Ra* r = −0.90; *Rz* r = −0.99) and Cr (*Ra* r = −0.71; *Rz* r = −0.91) exhibited very strong negative correlations, while Mo also followed this trend with *Ra* (r = −0.74) and *Rz* (r = −0.50). These results indicate that higher roughness is associated with depletion of protective alloying elements, whereas smoother surfaces retain more favourable compositions. These observations are consistent with the fact that, although emulsion produced the smoothest surface, roughness alone is not decisive for corrosion performance; the chemical state of the surface and the stability/composition of the passive film can outweigh pure topographic effects [29]. In line with prior work, machining-induced surface integrity (chemistry, residual stresses, near-surface defects) can dominate the electrochemical response even when Ra is low, explaining the slightly higher corrosion rates for the emulsion condition [30]. Overall, the analysis suggests that before corrosion, passivation is enhanced by higher Ni, Mo, and O contents together with smoother topography, while Fe, Si, and C enrichment, accompanied by increased roughness, undermines the stability of the passive film [19,25,29].

i.) Correlation after corrosion

To further examine the link between local chemical composition and corrosion degradation, Pearson correlation coefficients were calculated between the post-corrosion surface composition and destructive electrochemical parameters (E_{corr}, i_{corr}, corrosion rate). The analysis focused on the pit edge zone, considered the most representative for quantifying these relationships due to its intermediate character between passive and actively corroded areas [27,28]. A visual representation of the correlations is provided in the bar chart of Figure 12.

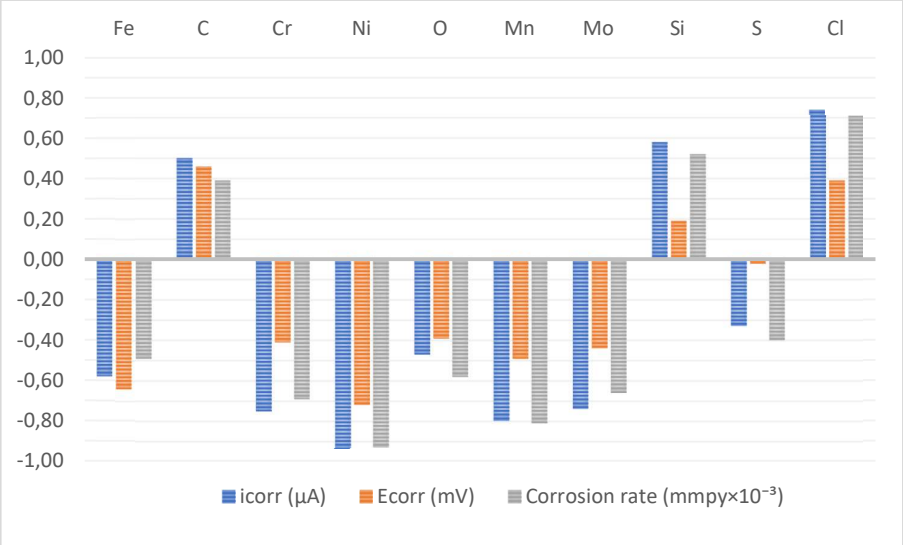

Figure 12. Bar chart of correlations between surface composition after corrosion and destructive electrochemical parameters.

Nickel exhibited the strongest negative correlations with i_{corr} (r = −0.94) and corrosion rate (r = −0.93). This confirms that Ni depletion directly destabilizes the passive film and increases reactivity, with samples containing the lowest Ni showing the most intense degradation [25]. Chromium displayed a similar trend, correlating negatively with i_{corr} (r = −0.75) and corrosion rate (r = −0.69), underlining its essential function in maintaining a continuous and stable passive layer. This aligns with reports linking Cr depletion to increased susceptibility to localized and intergranular corrosion [1]. Molybdenum also correlated negatively with destructive parameters (i_{corr} r = −0.74; corrosion rate r = −0.66), confirming its role in suppressing localized corrosion in chloride-rich environments [28]. Manganese showed consistently strong negative correlations (i_{corr} r = −0.80; corrosion rate r = −0.81), suggesting that although present in lower amounts, Mn contributes to stabilizing the passive film by reducing the tendency towards localized breakdown. Iron also demonstrated negative correlations (i_{corr} r = −0.58; corrosion rate r = −0.49). These results should be interpreted with caution, since Fe dominates the alloy matrix and its relative increase after corrosion generally reflects the depletion of alloying elements rather than indicating an inherently protective effect [19]. In contrast, carbon exhibited positive correlations with i_{corr} (r = 0.50) and corrosion rate (r = 0.39). This behavior likely reflects contamination by organic residues or the accumulation of corrosion byproducts that promote localized attack. Elevated carbon was especially pronounced in MQL-treated samples, supporting the interpretation that lubricant residues weaken passivation [12]. A similar mechanism may also explain the behaviour of the emulsion condition, where residual traces of the cooling fluid could have formed a thin organic film that hindered uniform passive layer development and delayed full passivation. Brinksmeier et al. [8] reported that certain emulsion additives and reaction products can locally interfere with oxide formation and modify electrochemical response. Chlorine showed strong positive correlations with i_{corr} (r = 0.74) and corrosion rate (r = 0.71), clearly identifying Cl as the most aggressive species in destabilizing the passive layer and promoting localized corrosion attack. Other elements, such as Si (i_{corr} r = 0.58; corr. rate r = 0.52) and S (i_{corr} r = −0.33; corr. rate r = −0.40), exhibited weaker correlations, suggesting a limited or non-protective role in the post-corrosion state [30].

4 Conclusion

The conducted study confirmed that the applied cooling and lubrication strategy during machining has a decisive influence on the corrosion behaviour of AISI 316L stainless steel. Dry machining consistently resulted in the poorest performance, with the lowest open circuit potentials, reduced polarization resistance, and the highest corrosion rates. In contrast, conventional emulsion cooling provided stable surface quality and improved electrochemical protection by supporting passive film stabilization [15], [12]. Minimum quantity

lubrication (MQL) alone showed limitations due to elevated surface carbon and reduced concentrations of passivating elements, which coincided with lower electrochemical stability [7], [22]. However, when combined with vortex tube cooling, MQL demonstrated significant improvements: despite higher surface roughness, this hybrid approach achieved the lowest overall corrosion rates and favourable open circuit potentials, indicating enhanced passivation efficiency [16], [12]. The integrated SEM/EDS and correlation analyses revealed that localized corrosion develops through selective depletion of chromium, nickel, and molybdenum at pit sites, while simultaneous enrichment with carbon and chloride promotes breakdown of passivity [17], [28]. Among the examined regions, the pit edge proved most representative for interpreting localized degradation, as it captured both early loss of protective elements and redistribution phenomena [25], [18]. Overall, the results highlight that MQL combined with vortex tube cooling represents a sustainable and efficient alternative to conventional emulsion, providing a favourable balance between corrosion resistance and ecological responsibility. Nevertheless, the performance of emulsion cooling remains the most predictable and uniform across all examined parameters. Future investigations should focus on optimizing lubricant formulations, extended immersion testing, and surface-sensitive analyses to clarify localized effects and refine sustainable machining strategies [24], [30].

Acknowledgments

This work has been partially supported by University of Rijeka, grant number uniri-mladi-technic-23-26 and grant number uniri-iskusni-tehnic-23-293.

References

[1] Matula, M., Hyspecka, L., Svoboda, M., Vodarek, V., Dagbert, C., Galland, J., Stonawska, Z., Tuma, L. *Intergranular corrosion of AISI 316L steel.* Materials Characterization, 46 (2-3) (2001), 203-210. https://doi.org/10.1016/S1044-5803(01)00125-5

[2] SreeMetaliks. *A Comprehensive Guide to 316L Stainless Steel: The Differences, Properties, and Benefits.* Available online: https://sreemetaliks.com/blog/a-comprehensive-guide-to-316l-stainless-steel-the-differences-properties-and-benefits. (accessed 10 June 2024)

[3] Kopac, J., Pusavec, F. *Concepts of Sustainable Machining Processes.* 13th International Research/Expert Conference "Trends in the Development of Machinery and Associated Technology" TMT 2009, Hammamet, Tunisia (2009). (accessed 10 June 2025).

[4] Sohrabi M.J., Mirzadeh H., & Dehghanian C. *Unraveling the effects of surface preparation on the pitting corrosion resistance of austenitic stainless steel.* Archiv.Civ.Mech.Eng, 20(8) (2020). https://doi.org/10.1007/s43452-020-0010-z.

[5] Rede, V. *Nehrđajući čelici.* Sveučilište u Zagrebu, FSB, Zagreb (2017).

[6] British Stainless Steel Association (BSSA). *General principles of machining stainless steels.* https://bssa.org.uk/bssa_articles/general-principles-of-machining-stainless-steels/. (accessed 10 June 2025).

[7] Lawal S.A. *A review of application of vegetable oil-based cutting fluids in machining non-ferrous metals.* Indian Journal of Science and Technology, 6(1) (2013): 3951-3956. DOI: 10.17485/ijst/2013/v6i1.22.

[8] Brinksmeier E., Meyer D., Huesmann-Cordes A.G., Herrmann C. *Metalworking fluids – Mechanisms and performance.* CIRP Annals – Manufacturing Technology, 64(2) (2015): 605-628. https://doi.org/10.1016/j.cirp.2015.05.003.

[9] Schwarz F. et al. *Health risks associated with inhalation of aerosols from metalworking fluids.* Report, University of Michigan, USA, (2015).

[10] Bierma T.J., Waterstraat F.L. *Total cost of ownership for metalworking fluids.* Report of Illinois Waste Management and Research Center, Illinois State University, USA, (2004).

[11] Liew, P.J., Hashim, U.S., Rahman, M.N.A. *Effect of chilled air coolant on surface roughness and tool wear when machining 2205 duplex stainless steel*. J. Adv. Manuf. Technol., 11 (2017), 61–68

[12] Šterpin Valić, G., Kostadin, T., Cukor, G., Fabić, M. *Sustainable Machining: MQL Technique Combined with the Vortex Tube Cooling When Turning Martensitic Stainless Steel X20Cr13.* Machines, 11(33) (2023). https://doi.org/10.3390/machines11010033.

[13] Thornburg, J., Leith, D. *Size distribution of mist generated during metal machining*. Appl. Occup. Environ. Hyg., 15 (2000), 618–628. doi: 10.1080/10473220050075626.
[14] Loto R.T., Loto C.A. *Potentiodynamic Polarization Behavior and Pitting Corrosion Analysis of 2101 Duplex and 301 Austenitic Stainless Steel in Sulfuric Acid Concentrations.* J Fail. Anal. and Preven., 17 (2017): 672-679. https://doi.org/10.1007/s11668-017-0291-6.
[15] Lv S., Yang Z., Zhang B. et al. *Corrosion and passive behavior of duplex stainless steel 2205 at different cooling rates in a simulated marine environment solution.* J. Iron Steel Res. Int., 25 (2018): 943-953. https://doi.org/10.1007/s42243-018-0136-x.
[16] Kostadin T. *Effect of Cooling with Cold Compressed Air on the Corrosion Resistance of Machined Parts Made of Stainless Steel.* Doctoral Thesis, University of Rijeka, (2019).
[17] DelVecchio, E., Liu, T., Chang, Y., Nie, Y., Eslami, M., Charpagne, M. A. *Metastable cellular structures govern localized corrosion damage development in additive manufactured stainless steel.* npj Materials Degradation, 8 (2024), 45. https://doi.org/10.1038/s41529-024-00464-8.
[18] Zhang, H., Huang, W., Wei, H., Chen, Z., Cao, J., Tang, Y., Zhao, X., Zuo, Y. *Effect of HAc on the Metastable Pitting Corrosion of 304 SS in NaCl Solution.* Materials, 15 (2022), 3618. https://doi.org/10.3390/ma15103618.
[19] Burstein, G. T., Pistorius, P. C. *Surface Roughness and the Metastable Pitting of Stainless Steel in Chloride Solutions.* CORROSION, 51 (5) (1995), 380–385. https://doi.org/10.5006/1.3293603.
[20] De Oliveira Jr., C.A., Diniz, A.E., Bertazolli, R. *Correlating tool wear, surface roughness and a corrosion resistance in the turning process of super duplex stainless steel.* Journal of Brazilian Society of Mechanical Sciences and Engineering, 36(4) (2014): 775-785. DOI: 10.1007/s40430-013-0119-6.
[21] Bueno, M.J., Borges, D.B.V., Mansur, F.A., Schvartzman, M.M.M.A. *Analysis of pitting corrosion in super martensitic stainless steel with different surface roughness in seawater.* 22 CBECiMat - Congresso Brasileiro de Engenharia e Ciência dos Materiais, Natal, RN, Brasil (2016): 6640-6651.
[22] Cukor, G., Šterpin-Valić, G., Kostadin, T., Fabić, M.. *Sustainable Turning of Martensitic Stainless Steel*. Transactions of FAMENA, 43 (3) (2019). https://doi.org/10.21278/TOF.43301.
[23] Gamry Instruments. Electrochemical Corrosion Measurements. Available online: https://www.gamry.com/assets/Uploads/Electrochemical-Corrosion-Measurements.pdf (accessed 10 June 2024).
[24] Malik, A.U., Kutty, P.C.M., Siddiqi, N.A., Andijani, I.N., Ahmed, S. *The Influence of pH and Chloride Concentration on the Corrosion Behaviour of AISI 316L Steel in Aqueous Solutions.* Corrosion Science, 33 (11) (1992): 1809-1827.. DOI: 10.1016/0010-938X(92)90011-Q
[25] Clark, R.N., Chan, C.M., Walters, W.S., Engelberg, D., Williams, G. *Intergranular and Pitting Corrosion in Sensitized and Unsensitized 20Cr–25Ni–Nb Austenitic Stainless Steel.* Corrosion, 77 (2021), 552–563. https://doi.org/10.5006/3725.
[26] Grandy, L., Yassine, S. R., Lacasse, R., Mauzeroll, J. *Selective Initiation of Corrosion Pits in Stainless Steel Using Scanning Electrochemical Cell Microscopy.* Anal. Chem., 96 (2024), 7394–7400. https://doi.org/10.1021/acs.analchem.3c04637.
[27] Sedriks, A.J. *Corrosion of Stainless Steels*, 2nd ed.; Wiley: New York, NY, USA, (1996): 242–244.
[28] Sun Q, Xie F, Zhang Y, Wang D, Wu M. *Stability of passive film and pitting susceptibility of 316L stainless steel in the aggressive oilfield environment containing Cl^-–CO_2–O_2.* Electrochim Acta., 499 (2024). https://doi.org/10.1016/j.electacta.2024.144709.
[29] Vadiraj, A., Kamaraj, M. *The Effect of Surface Roughness on the Corrosion Properties of Type AISI 304 Stainless Steel in Diluted NaCl and Urban Rain Solution.* J. Mater. Eng. Perform., 19 (2010), 761–765. https://doi.org/10.1007/s11665-009-9549-y
[30] Wang, S., Hu, Y., Fang, K., Zhang, W., Wang, X. *Effect of surface machining on the corrosion behaviour of 316 austenitic stainless steel in simulated PWR water.* Corrosion Science, 126 (2017), 104-120. DOI: 10.1016/j.corsci.2017.06.019